JOURNAL OF CATALYSIS **162,** 306–319 (1996)
ARTICLE NO. 0288

Tungsten–Oxo-Species Deposited on Alumina

II. Characterization and Catalytic Activity of Unpromoted $W^{(vi)}/\gamma$-Al_2O_3 Catalysts Prepared by Equilibrium Deposition Filtration (EDF) at Various pH's and Non-Dry Impregnation (NDI)

L. Karakonstantis, H. Matralis, Ch. Kordulis, and A. Lycourghiotis[1]

Department of Chemistry, University of Patras-Institute of Chemical Engineering and High Temperature Chemical Processes, ICE/HT-FORTH-Hellas, P.O. Box 1414, GR.-265 00, Patras, Greece

Received October 5, 1995; revised April 5, 1996; accepted April 15, 1996

A series of $W^{(vi)}/\gamma$-Al_2O_3 catalysts of varying $W^{(vi)}$ content in the range 3.3–21.2% WO_3 was prepared at various pH's using equilibrium deposition filtration (EDF).These catalysts were then characterized using various physicochemical techniques (BET, XPS, XRD, DRS, NO chemisorption, TPD of NH_3, microelectrophoresis, and DTGA) and the surface characteristics achieved were related with the nature of the $W^{(vi)}$ species deposited on the γ-alumina surface during preparation. A close relation exists between the nature of the deposited $W^{(vi)}$ species and the structure and dispersity of the $W^{(vi)}$-supported phase: Deposition through adsorption or reaction of the *monomeric* WO_4^{2-} species in the pH range 7.4–4.9 resulted in a well-dispersed, presumably monolayered, $W^{(vi)}$ phase relatively rich in tetrahedral $W^{(vi)}$. In contrast, deposition through adsorption of the *polymeric* $HW_6O_{20}(OH)_2^{5-}$ species at pH's 4.0 and 3.5 resulted in a supported phase with relatively low dispersity and a relatively small amount of tetrahedral $W^{(vi)}$. Supported WO_3 crystallites with size greater than 40 nm are formed in this case. Moreover, it was inferred that the mode of deposition of the monomeric WO_4^{2-} species is reflected in the properties of the supported $W^{(vi)}$ phase of the calcined samples. Thus, TPR and NO chemisorption data strongly suggested that the change in the deposition mechanism (upon decreasing pH from 6.1 to 4.9) from deposition through surface reaction of the monomeric WO_4^{2-} species with neutral hydroxyls of the support into deposition through adsorption of these species on protonated surface hydroxyls of the support brought about a decrease in the "supported phase-carrier" interactions as well as an increase in the surface of the supported $W^{(vi)}$. Three catalysts with $W^{(vi)}$ loading corresponding to that of the three EDF catalysts (3.3, 11, and 21.2% WO_3/γ-Al_2O_3) were also prepared using the usual methodology of nondry impregnation (NDI) and characterized using the aforementioned techniques. It was found that NDI resulted in a supported phase with lower dispersity and less rich in tetrahedral $W^{(vi)}$ species than EDF. Moreover, catalytic tests, using the hydrodesulfurization of thiophene and the hydrogenation of cyclohexene as probe reactions, showed that EDF provides more active catalysts than NDI and this is another example showing that EDF with controlled regulation of the impregnation parameters is a promising methodology for preparing supported catalysts even with relatively low loadings. Finally, it was found that EDF provides more acidic samples than NDI.

INTRODUCTION

In the first article of this series we reported on the mechanism of deposition of the $W^{(vi)}$ species from aqueous solutions on the γ-alumina surface (1). Adopting the 2p*K*/one-site model for the γ-alumina surface and the triple-layer model for the double-layer developed between the support surface and the electrolyte solution we were able to develop a detailed deposition model (1). This tentative model, based on experimental results previously reported (2), was then tested by three independent ways: First by comparing calculated and experimental deposition isotherms, second by comparing the expected, according to the model, and the experimentally determined disturbance in the ability of the support to adsorb H^+ ions due to the presence of the $W^{(vi)}$ species in the solution, and third by comparing the model and the experimental variation of the ζ-potential with pH. The aforementioned procedure showed that, although in the impregnating solution 12 different $W^{(vi)}$ species are present, the deposition mechanism is rather simple:

$$AlOH_2^+ + WO_4^{2-} \longleftrightarrow AlOH_2^+ \ldots WO_4^{2-} \quad [1a]$$

$$AlOH_2^+ + HW_6O_{20}(OH)_2^{5-} \longleftrightarrow AlOH_2^+ \ldots HW_6O_{20}(OH)_2^{5-} \quad [1b]$$

$$AlOH + WO_4^{2-} \longleftrightarrow Al\text{–}O\text{–}(WO_3)^- + OH^- \quad [1c]$$

$$2AlOH + WO_4^{2-} \longleftrightarrow Al\text{–}O\text{–}(WO_2)\text{–}O\text{–}Al + 2OH^-. \quad [1d]$$

According to this mechanism the deposition of the $W^{(vi)}$ species on the γ-alumina surface takes place by adsorption of the WO_4^{2-} and $HW_6O_{20}(OH)_2^{5-}$ on sites created in the inner Helmholtz plane (IHP) of the double layer by single

[1] To whom correspondence should be addressed.

0021-9517/96 $18.00

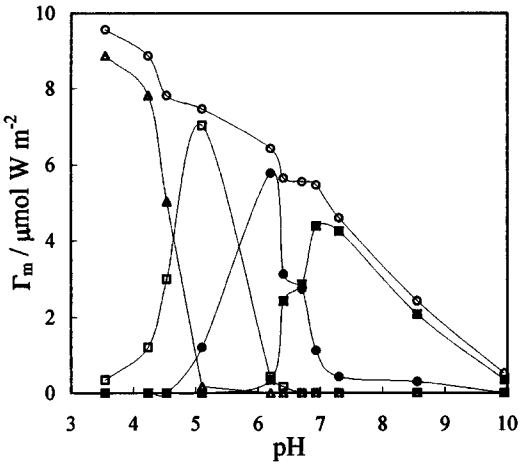

FIG. 1. Variation with pH of the maximum amount of W deposited on the surface of γ-alumina. (■) Deposition via reaction of the monomeric WO_4^{2-} with two neutral surface hydroxyls (equilibrium [1d]). (●) Deposition via reaction of the monomeric WO_4^{2-} with one neutral surface hydroxyl (equilibrium [1c]). (□) Deposition via adsorption of monomeric WO_4^{2-} ion on a site created in IHP by one protonated surface hydroxyl of the support (equilibrium [1b]). (△) Deposition via adsorption of the polymeric $HW_6O_{20}(OH)_2^{5-}$ species on a site created in the IHP by one protonated surface hydroxyl of the support (equilibrium [la]). (○) "Total" deposition via equilibria [1].

protonated surface hydroxyls as well as by reaction of the WO_4^{2-}species with a single or a pair of adjacent neutral hydroxyls.

The most important achievement of the work reported in the first article of this series was the establishment of the variation of the concentration of the $W^{(vi)}$ species formed on the support surface with the pH of the impregnating solution. This variation, illustrated in Fig. 1, corresponds to the plateau of the deposition isotherms. It may be observed that in the pH range 10–7, the deposition takes place practically by reaction of the monomeric WO_4^{2-} species with two adjacent AlOH groups. As pH decreases, the deposition by reaction of the WO_4^{2-} with the single AlOH groups becomes more and more important. The concentration of the $Al–O–(WO_3)^-$ is maximized at about pH 6 and then rapidly decreased. Further decrease in the pH promotes the deposition by adsorption of the WO_4^{2-} ions. It may be seen that the extent of the first equilibrium is maximized at pH near 5. In the pH range 4.5–3.5 the deposition by adsorption of the polymeric $HW_6O_{20}(OH)_2^{5-}$ becomes important.

The elucidation of the deposition mechanism and the possibility of knowing the concentrations of the $W^{(vi)}$ species formed on the support surface at each pH offers a unique opportunity to investigate whether there is any relation between the $W^{(vi)}$ species mentioned and the surface properties of the $W^{(vi)}/\gamma$-Al_2O_3 catalysts that are important from the viewpoint of catalysis. Although many studies have been devoted mainly to the characterization of the $W^{(vi)}/\gamma$-Al_2O_3 catalysts (3–34), attempts to relate the surface properties of the calcined samples with the kind and concentration of the deposited W species on the support surface are almost nonexistent. This is because in most cases the $W^{(vi)}/\gamma$-Al_2O_3 catalysts were prepared by dry or nondry impregnation followed by drying. In these cases the deposition of the $W^{(vi)}$ on the support surface takes place mainly by precipitation in the step of drying, a process extremely difficult to model. Even in the few cases where the preparation was performed by equilibrium deposition followed by filtration (EDF) (2, 3, 7, 9, 33, 34), the absence of any information concerning the detailed deposition mechanism rendered extremely difficult to investigate the relation between the surface properties of the calcined samples and *the nature* of the surface species formed on the support surface during impregnation.

The investigation of the aforementioned relation is the principal goal of the present work. Specifically, we prepared, using EDF, several $W^{(vi)}/\gamma$-Al_2O_3 catalysts of varying $W^{(vi)}$ content by depositing the $W^{(vi)}$ species at selected pH values. These catalysts were then characterized using various physicochemical techniques (X-ray photoelectron spectroscopy, diffuse reflectance spectroscopy, NO chemisorption, X-ray powder diffraction, temperature-programmed reduction, microelectrophoresis, temperature-programmed desorption of ammonia, and differential thermogravimetry) and the surface properties achieved were related to the nature of the $W^{(vi)}$ species deposited on the support surface during preparation. A second goal of the present work is to compare the surface and catalytic properties of catalysts prepared by EDF with the corresponding properties of catalysts, with the same $W^{(vi)}$ loading, prepared by the classical technique of the nondry impregnation (NDI) followed by drying. To compare the surface properties we prepared and characterized, using the forementioned methods, three additional NDI catalysts. To compare the catalytic activity of the catalysts prepared by EDF and NDI we carried out catalytic tests on some EDF and NDI catalysts using the hydrodesulfurization of thiophene and the hydrogenation of cyclohexene as probe reactions. The coke formation on the aforementioned samples during aging and testing has finally been determined. The second goal of the present work is related to our effort to develop the EDF methodology for preparing supported catalysts.

EXPERIMENTAL

Materials

γ-Alumina was used as a support in the present work. It was obtained by crushing γ-alumina extrudates purchased from Houndry (Ho 415 γ-alumina extrudates, $SSA_{BET} = 131\ m^2\ g^{-1}$, water pore volume: $0.45\ cm^3\ g^{-1}$). The crushed

extrudates were sieved and a fraction between 100–150 mesh was selected. This was impregnated with bidistilled water, dried at 120°C for 2.5 h, and then air calcined at 600°C for 12 h.

Ammonium tungstate [$(NH_4)_{12}W_{12}O_{41}5H_2O$, 99.999%] purchased from Ventron was used for the preparation of the tungstate aqueous solutions necessary in the synthesis of the $W^{(vi)}/\gamma$-Al_2O_3 specimens. Ammonium nitrate (NH_4NO_3, Riedel de Haen, 99%) was used for the preparation of the aqueous solutions of the background electrolyte. These solutions were used in turn for regulating the ionic strength of the tungstate solutions.

Preparation of the $W^{(vi)}/\gamma$-Al_2O_3 Specimens

Two methods were followed for depositing the $W^{(vi)}$ species on the support surface: equilibrium deposition filtration (EDF) and NDI. Following the first methodology an amount of the γ-alumina powder equal to 8.0 g was added into a tungstate solution of 1.6×10^{-2} mol $W^{(vi)}$ dm^{-3} totaling 2.240 dm^3. In all cases studied the ionic strength of the solution was adjusted to 0.16 *M* using NH_4NO_3. The pH of the suspension was regulated using HNO_3 or NH_4OH. After stirring for 20 h at 25°C, the suspension was filtered using membrane filters (Millipore, 0.22 μm). The solid was dried at 120°C for 2.5 h. Then a portion of the solid was air calcined at 300°C for 1 h and then at 600°C for 6 h. The $W^{(vi)}$ content in the EDF specimens was determined using UV spectroscopy (35). Following the second methodology (NDI) an amount of $(NH_4)_{12}W_{12}O_{41}5H_2O$ calculated to correspond to the amount of the $W^{(vi)}$ to be deposited was dissolved in 50–100 ml bidistilled water containing 8.0 g of γ-Al_2O_3 and the solvent was progressively evaporated using a rotary evaporator. A portion of the solid was air calcined at 300°C for 1 h and at 600°C for 6 h. The EDF and NDI prepared specimens are compiled in Table 1.

The filtrates resulted from the various impregnations were selected and the solvent was removed by evaporation provoking the precipitation of a solid, presumably $(NH_4)_{12}W_{12}O_{41}$ $5H_2O$. After filtration the precipitate was dried at 120°C for 2.5 h and then it was air calcined at 670–700°C for 7 h. The product, identified by XRD to be WO_3, was used as standard in the present study.

Characterization of the Specimens

The specimens prepared were characterized using various physicochemical techniques: (i) N_2 adsorption to determine the specific surface area, (ii) X-ray photoelectron spectroscopy (XPS) to investigate the dispersity, or the surface, of the supported $W^{(vi)}$, (iii) X-ray powder diffraction (XRD) to identify the $W^{(vi)}$ species formed on the support surface, (iv) diffuse reflectance spectroscopy (DRS) to investigate the symmetry and the valence of the supported tungsten, (v) temperature-programmed reduction (TPR) to investigate the supported species and the "active phase-carrier interaction", (vi) NO chemisorption to estimate the surface of the supported $W^{(vi)}$, (vii) temperature-programmed desorption of NH_3 (NH_3-TPD) and microelectrophoresis to investigate the acidity of the samples, and (viii) differential thermogravimetry (DTGA) to investigate the $W^{(vi)}$ species formed during the NDI and EDF preparation. Experimental details concerning the aforementioned characterization techniques have been reported in our previous publications (36–38). It should be noted that all characterizations except DTGA have been performed on calcined samples.

TABLE 1

Compiles the Surface Areas per Gram of the Support, SSA, and per Gram of Catalysts, $\overline{SSA}$, for the Specimens Prepared by EDF, at Various pH's and by NDI

Specimen	Methodology	Equilibrium pH	SSA	$\overline{SSA}$
3.3% WO_3/γ-Al_2O_3	EDF	7.0[a]	113	109
11.0% WO_3/γ-Al_2O_3	EDF	7.4	127	113
13.9% WO_3/γ-Al_2O_3	EDF	6.1	144	124
17.3% WO_3/γ-Al_2O_3	EDF	4.9	119	99
19.9% WO_3/γ-Al_2O_3	EDF	4.0	117	94
21.2% WO_3/γ-Al_2O_3	EDF	3.5	132	104
3.3% WO_3/γ-Al_2O_3	NDI	—	128	124
11.0% WO_3/γ-Al_2O_3	NDI	—	102	87
21.2% WO_3/γ-Al_2O_3	NDI	—	105	82
γ-Al_2O_3	—	—	131	—
WO_3	—	—		3

[a] This sample was prepared using impregnating solution of $W^{(vi)}$ with concentration equal to 10^{-3} mol $W^{(vi)}$ dm^{-3} and ionic strength equal to 0.16 *M* NH_4NO_3.

Catalytic Activity Measurements and Determination of the Carbon Deposition

Catalytic activity was measured for some of the samples prepared using the hydrodesulfurization of thiophene and the hydrogenation of cyclohexene as probe reactions. A conventional flow apparatus equipped with a Pyrex glass reactor operating in differential mode under atmospheric pressure has been used. The samples were presulfided *in situ*, with a stream of 15% v/v hydrogen sulfide in hydrogen, for 2.5 h at 400°C. The reaction mixture fed to the reactor with flow rates in the range 3–55 ml min^{-1} to ensure differential operation. After an aging period of 15 h under the stream of the reaction mixture the rates of the aforementioned reactions were determined. A gas chromatograph (Pye Unicam) equipped with a flame ionization detector and a column (8 m, 1/8 in. o.d.) filled with carbowax 20M on chromosorb P. A.W. was used to analyze the effluent of the reactor. Spent samples were analyzed for carbon deposited during the activity tests using a carbon analyzer (EA 1108, Carlo Erba Strumentazione).

RESULTS AND DISCUSSION

Specific Surface Area

Table 1 compiles the values of the surface area per gram of γ-alumina (denoted by SSA) and per gram of catalysts (denoted by $\overline{\text{SSA}}$) determined for the specimens prepared. Concerning the EDF specimens it is clear that the texture of the support is not affected by the formation of the $W^{(vi)}$ species on its surface. Taking into account the accuracy of the BET technique, all the SSA values achieved are practically equal to that obtained for the support. This may be easily explained. In fact, whereas the surface concentration of $W^{(vi)}$ deposited *by precipitation in the step of drying*, which follows the filtration, was calculated to be equal to $(0.12–5) \times 10^{-2}$ μmol $W^{(vi)}$ m^{-2}, the surface concentration of $W^{(vi)}$ deposited *by reaction or adsorption in the step of impregnation* was calculated to be in the range 1.2–9.4 μmol $W^{(vi)}$ m^{-2} (1). The deposition in the step of impregnation by adsorption or surface reaction is expected to result in a very thin supported layer of the $W^{(vi)}$ species or very thin supported crystallites. This situation does not favor the sintering of the supported crystallites and the subsequent closing of the thin pores of the support.

In contrast to the above, the SSA values achieved for the specimens prepared by NDl with $W^{(vi)}$ loading equal to 11 and 21.2% WO_3 are lower than the corresponding values achieved for the EDF samples. This suggests the formation of larger supported crystallites in these NDI samples, which might provoke a partial closing of the thin pores of the support. This may be attributed to the fact that the principal mode of deposition in the NDI samples *is the precipitation in the step of drying which follows impregnation*. In fact, in the NDI samples the time required for the evaporation of the solvent is considerably shorter (0.45–1.5 h) than that required to attain the equilibria [1] (1). Moreover, the impregnating solution used for preparing the NDI samples are more concentrated (2.5×10^{-2} *M*, 6.1×10^{-2} *M*, 9.8×10^{-2} *M*) than those used for the preparation of the EDF samples (1.6×10^{-2} *M*).

As to the considerable decrease in the $\overline{\text{SSA}}$ values observed in both the EDF and NDI specimens with respect to that achieved for the support, it may be easily attributed to the increase of the density of the samples after the formation of the $W^{(vi)}$ species on the γ-alumina surface.

X-Ray Photoelectron Spectroscopy

The above showed that the BET results offer the first evidence that EDF provides $W^{(vi)}/\gamma$-Al_2O_3 catalysts with a larger active surface than NDI. This is in full agreement with the XPS results illustrated in Fig. 2. Inspection of this figure clearly shows that the XPS intensity ratio $I_{W_{4f}}/I_{Al_{2p}}$, which is used to estimate the supported $W^{(vi)}$ surface (10, 24, 39), is larger in the EDF than in the corresponding NDI specimens. The difference increases with the $W^{(vi)}$ loading. This is rather expected because the portion of the $W^{(vi)}$ deposited by precipitation in the NDI specimens should be increased with the $W^{(vi)}$ concentration of the impregnating solution.

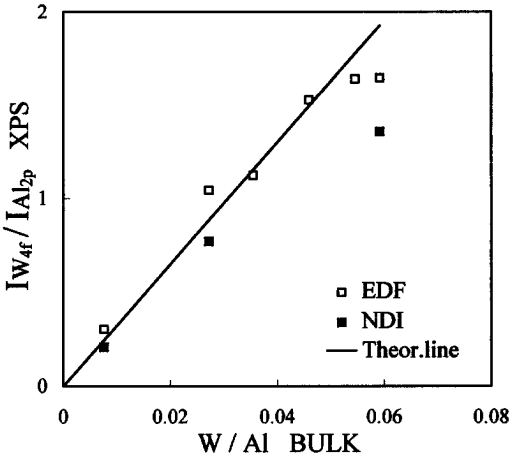

FIG. 2. Intensity ratio, $I_{W_{4f}}/I_{Al_{2p}}$, of the W_{4f} and Al_{2p} photoelectrons, used to estimate the surface of the supported $W^{(vi)}$, against the bulk atomic ratio W/Al. The calculated solid line is based on the model of Kerkhof and Moulijn (40, 41).

Let us now concentrate our attention on the EDF samples. Figure 2 shows a linear increase in the $I_{W_{4f}}/I_{Al_{2p}}$ ratio up to the sample containing 17.3% WO_3. Up to this concentration the calculated solid line based on the model of Kerkhof and Moulijn (40) describes quite well our experimental points, indicating almost monolayered structure for the supported phase (40). This very favorable structure, from the viewpoint of catalysis, may be easily related to the nature of the species deposited on the γ-alumina surface during impregnation. In fact, the EDF samples with $W^{(vi)}$ content in the range 3.3–17.3% WO_3 have been prepared in the pH range 7.5–4.9 when *only* the monomeric WO_4^{2-} species are deposited on the γ-alumina surface (see Fig. 1). These species seem to be responsible for the formation of an almost monolayered supported phase. Decrease in the pH of the impregnating suspension below 4.9 brings about the deposition of the polymeric $HW_6O_{20}(OH)_2^{5-}$ species on sites created in the IHP by single $AlOH_2^+$ groups. This, in turn, causes an increase of the $W^{(vi)}$ content in the calcined samples. Both phenomena, *not only the second one traditionally considered to be the unique reason*, should be responsible for the decrease in the $I_{W_{4f}}/I_{Al_{2p}}$ ratio and the deviation from the structure of the supported phase mentioned above. In fact, careful inspection of Fig. 1 shows that in the EDF samples with $W^{(vi)}$ equal to 19.2 and 21.2% WO_3, which have been prepared at pH's 4.0 and 3.5, respectively, almost all the $W^{(vi)}$ has been deposited *via* adsorption of the $HW_6O_{20}(OH)_2^{5-}$ species. Specifically, it was calculated (2) that 83 and 91% of the tungsten is deposited *via* the

equilibrium [1b] at pH's 4.0 and 3.5, respectively. The very strong lateral interactions exerted between these species (2) and the high density of the supported phase in $W^{(vi)}$ would facilitate the formation of surface multilayers and supported (bulk) WO_3 upon calcination, justifying thus the decrease in the $W^{(vi)}$ dispersity. In this point it should be noted that calculations using SURFEQL (2) show negligible (very small) adsorption of the $HW_6O_{20}(OH)_2^{5-}$ ions on sites created by two adjacent groups at pH 4 (pH 3.5). Adsorption on sites created by more than two adjacent $AlOH_2^+$ groups does not occur. Moreover, these calculations show that only 21 and 18% of the total surface hydroxyls ($AlOH + AlOH_2^+ + AlO^-$) are covered by the aforementioned $W^{(vi)}$ species at pH's 4 and 3.5, respectively. The other remain free. In view of the above, we may imagine the adsorbed $HW_6O_{20}(OH)_2^{5-}$ ions to be accommodated vertically to the support surface above certain $AlOH_2^+$ groups. This indicates very high local concentration before heating, which as already mentioned is responsible for the formation of the surface $W^{(vi)}$ multilayers and supported WO_3 upon calcination. The deviation from the $I_{W_{4f}}/I_{Al_{2p}}$ vs $(W/Al)_b$ linearity above a critical $(W/Al)_b$ value, obviously depending on the preparation method and the specific surface area of the support, is in agreement with the literature (10).

X-Ray Powder Diffraction (XRD)

The above are fully confirmed by the XRD results (Figs. 3 and 4). In fact, on all the X-ray diffraction patterns of the specimens prepared peaks due to the crystalline γ-alumina have been detected (2θ: 37.39, 45.95, and 67.06°). On the other hand only on the EDF specimens with $W^{(vi)}$ content equal to 19.9 and 21.2% WO_3 and in the NDI specimen with the maximum $W^{(vi)}$ loading the characteristic triplet (2θ: 23.12, 23.60, and 24.38°) (41), which reveals the formation of crystalline WO_3, was detected. The XRD pattern of the EDF specimen with $W^{(vi)}$ content equal to 17.3% WO_3, prepared at pH 4.9, offers weak evidence, if any, for the formation of very small amounts of supported (bulk) WO_3. In this point it should be noted that the detection of crystalline WO_3 at $W^{(vi)}$ loading corresponding to about 5 atoms nm^{-2} is in full agreement with the literature (10). The lack of detection of the characteristic triplet for the crystalline WO_3 in the specimens with $W^{(vi)}$ loading lower than 19.9% WO_3 corroborates the picture drawn from the XPS results that in this $W^{(vi)}$ loading a monolayer structure or very thin supported crystallites (smaller than 40 nm) (42) are formed on the γ-alumina surface. However, the XPS strongly suggests that the magnitude of the "EDF supported crystallites," if any, is smaller than the corresponding NDI-supported crystallites.

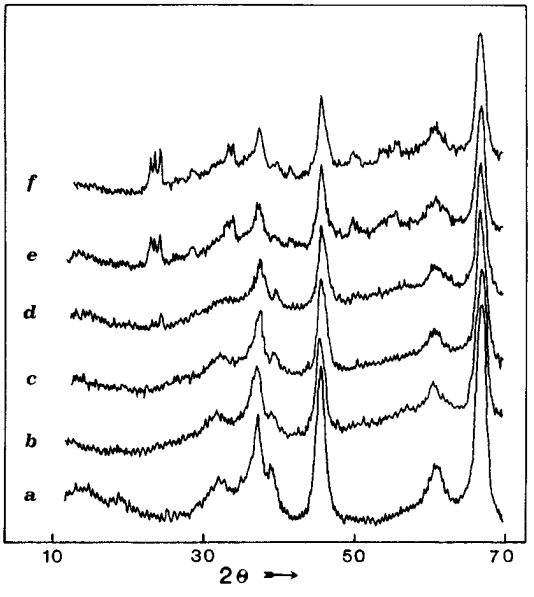

FIG. 3. X-ray diffraction spectra of the $W^{(vi)}/\gamma$-Al_2O_3 specimens prepared by EDF. (a) 3.3% WO_3, (b) 11% WO_3, (c) 13.9% WO_3, (d) 17.3% WO_3, (e) 19.9% WO_3, (f) 21.2% WO_3.

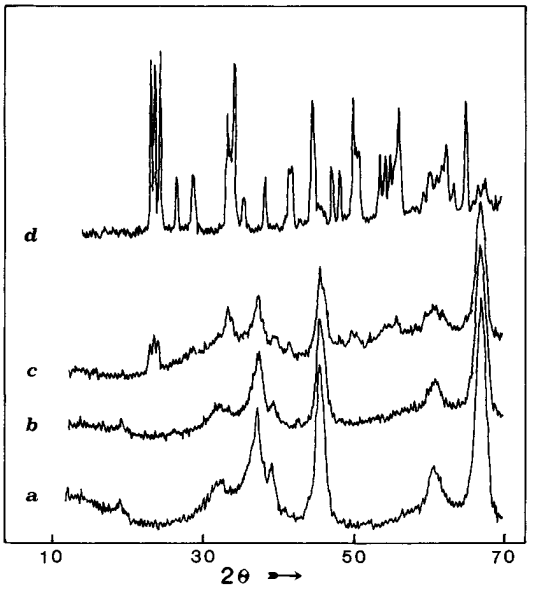

FIG. 4. X-ray diffraction spectra of the $W^{(vi)}/\gamma$-Al_2O_3 specimens prepared by NDI (a) 3.3% WO_3, (b) 11% WO_3, (c) 21.2% WO_3, (d) bulk WO_3.

Diffuse Reflectance Spectroscopy (DRS)

The above are also corroborated by the DRS results. Figure 5 illustrates the DR spectra of the model compounds used in the present study in the range 200–500 nm, namely the DR spectra of Na_2WO_4, $(NH_4)_{12}W_{12}O_{41}$ $5H_2O$, and WO_3. The $W^{(vi)}$ in Na_2WO_4 is in tetrahedral symmetry. According to the literature (4, 7, 8, 43) the $W^{(vi)}$ in this symmetry absorbs in the range 205–225 nm in agreement with the DR spectrum of the Na_2WO_4. $(NH_4)_{12}W_{12}O_{41}$ $5H_2O$ may be used as a model compound for the $W^{(vi)}$ in normal

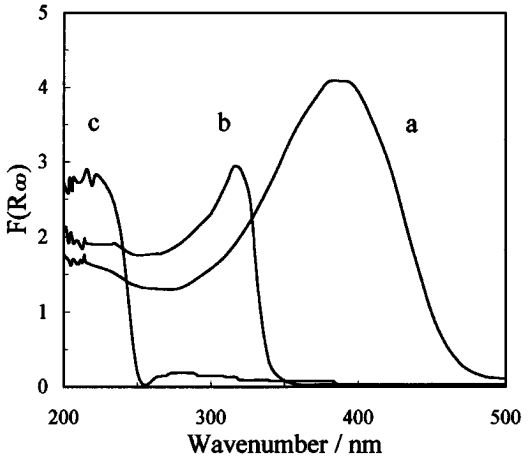

FIG. 5. Diffuse reflectance spectra recorded in the range 200–500 nm for the model compounds. (a) WO_3 (b) $(NH_4)_{12}W_{12}O_{41}\,5H_2O$, (c) Na_2WO_4. $F(R\,\infty)$ represents the Kubelca–Munk function.

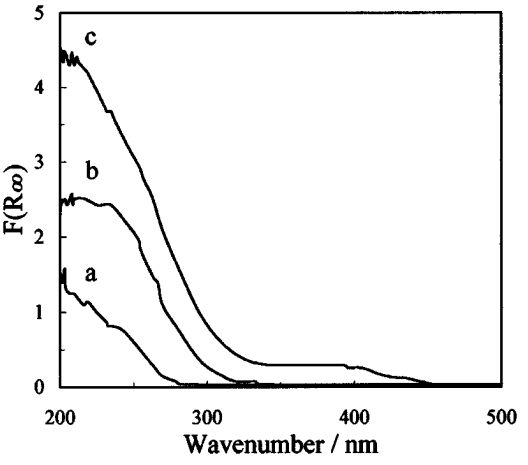

FIG. 7. Diffuse reflectance spectra recorded in the range 200–500 nm for the NDI specimens. (a) 3.3% WO_3, (b) 11% WO_3, (c) 21.2% WO_3. $F(R\,\infty)$ represents the Kubelca–Munk function.

octahedral symmetry. In fact, in this compound the ratio of tetrahedral to normal octahedral $W^{(vi)}$ is about 2/10. Inspection of the DR spectrum of the $(NH_4)_{12}W_{12}O_{41}\,5H_2O$ shows that the absorption of $W^{(vi)}$ in normal octahedral symmetry is centered at about 305–325 nm. The $W^{(vi)}$ in the WO_3 is mainly in the disturbed octahedral symmetry. It may be seen that the absorption band of WO_3 is maximized in the range 380–400 nm and this is in agreement with the literature (8).

Figures 6 and 7 illustrate the DR spectra recorded for the EDF and NDI catalysts, respectively. Figure 8 illustrates the variation, with the $W^{(vi)}$ loading of the value of the K–M function calculated at 215, 315, and 390 nm corresponding to the $W^{(vi)}$ in tetrahedral, normal, and distorted octahedral environment. The fact that the specimens prepared do not absorb in the range 400–800 nm indicates that the $W^{(vi)}$ species with valence lower than six are not practically formed on the support surface irrespectively of the methodology followed for depositing tungsten. This is in excellent agreement with our XPS results, which in all cases showed a binding energy equal to 35.9 ± 0.1 eV for the $W_{4f7/2}$ photoelectrons corresponding to $W^{(vi)}$ (10, 19, 21, 24).

Let us concentrate our attention on the EDF catalysts. Inspection of Fig. 8 shows that the tetrahedral $W^{(vi)}$ increases linearly up to 17.3% WO_3 and then it decreases. Moreover, at this $W^{(vi)}$ content, an articulation point may be observed for the curve describing the dependence of the $W^{(vi)}$ normal octahedral on the $W^{(vi)}$ content. Finally, after this $W^{(vi)}$ content starts the formation of the supported (bulk) WO_3

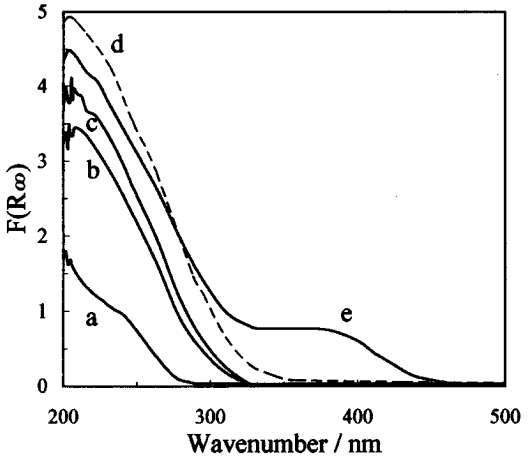

FIG. 6. Diffuse reflectance spectra recorded in the range 200–500 nm for the EDF specimens. (a) 3.3% WO_3, (b) 11% WO_3, (c) 13.9% WO_3, (d) 17.3% WO_3, (e) 19.9 or 21.2% WO_3. $F(R\,\infty)$ represents the Kubelca–Munk function.

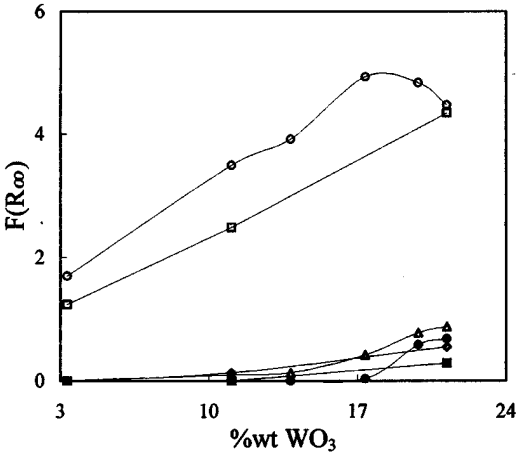

FIG. 8. Variation of the Kubelca–Munk function calculated at 215 nm (◯, EDF; □, NDI), 315 nm (△, EDF; ◇, NDI), and 390 nm (●, EDF; ■, NDI) with the $W^{(vi)}$ loading.

(see Figs. 5 and 7). These results, being in full agreement with our XPS and XRD results, *stress the very close relation between the nature of the* $W^{(vi)}$ *species deposited following EDF and the structure of the supported phase*. In fact, the only species deposited in the pH range 7–4.9, corresponding to the $W^{(vi)}$ loading 3.3–17.3% WO_3, *is the monomeric* WO_4^{2-} in which $W^{(vi)}$ is in tetrahedral symmetry (see Fig. 1).

At this point we might speculate on the nature of the $W^{(vi)}$ species formed on the calcined EDF catalysts with $W^{(vi)}$ in the range 3.3–17.3% WO_3. This speculation is based on our deposition results (Fig. 1, Eqs. [1d], [1c], and [1a]) as well as on our characterization results presented so far. The $W^{(vi)}$ species formed during impregnation in the pH range 7.4–4.9 corresponding to the samples 3.3–17.3% WO_3/γ-Al_2O_3 are illustrated in the right hand side of Eqs. [1d], [1c], and [1a]. Specifically, in the first and second specimens [3.3% WO_3/γ-Al_2O_3, 11% WO_3/γ-Al_2O_3] the species (I) and (II) are formed during impregnation.

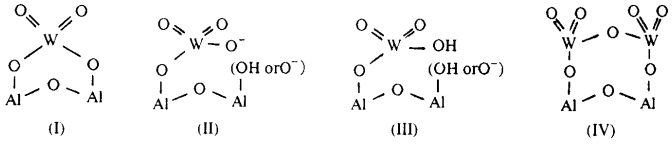

(I) 87 and 91% in the first and second sample, respectively.

(II) 13 and 9% in the first and second sample, respectively.

Species (I), being quite stable, is not expected to be transformed during heating (drying and calcination). For the species (II) there are three possibilities. First it can be transformed into species (III). Second, it might be dimerized, resulting in species (IV). Third it can be transformed into species (I) presumably via species (III). However, it seems reasonable to assume that the second possibility is less probable than the first. In fact, the dimerization requires the deposition of two negative $W^{(vi)}$ species on two adjacent AlOH groups. Taking into account that the formation of species (I) takes place exclusively on pairs of adjacent AlOH groups, we are inclined to believe that species (Il) are mainly formed on isolated AlOH groups. In view of the above it seems reasonable to claim that in the first and second calcined samples the species (I) (major species) and (III) (minor species) are formed. However, the formation of species (IV) cannot be excluded. The formation of these species, reported in the literature, even for specimens prepared by dry or nondry impregnation, are in excellent agreement with our characterization results stated so far (10, 34, 44). Concerning the DRS results it should be noted that the $W^{(vi)}$ in the species (I), (III), and (IV) is in tetrahedral symmetry. Going from the sample 11% WO_3/γ-Al_2O_3 (pH 7.4) to the sample 13.9% WO_3/γ-Al_2O_3 (pH 6.1) the situation is changed in the impregnation step. The species (II) is mainly formed during impregnation [species (I) 11%, species (II) 82%, $AlOH_2^+ \ldots WO_4^{2-}$ (17%)]. Therefore, species (III) and presumably species (I) and (IV) should predominate in the calcined 13.9% WO_3/γ-Al_2O_3 sample. Thus, the aforementioned change in the impregnation step cannot be detected in the calcined sample by BET, XRD, XPS, and DRS.

Let us finally examine the sample 17.3% WO_3/γ-Al_2O_3 (pH 4.9) in which the deposition of $W^{(vi)}$ still occurs via the monomeric species WO_4^{2-}. In this case the deposition takes place mainly via adsorption [$AlOH_2^+ \ldots WO_4^{2-}$, (94%), species (II) (6%)]. Moreover, in this case species (I) was not formed at all during impregnation. Taking into account that the formation of species (I) rendered quite difficult the deposition of WO_4^{2-} or the formation of species (II) *on adjacent* surface hydroxyls, a more "concentrated" $W^{(vi)}$ phase is now expected. This is corroborated by our calculations that showed that the percentage of the covered (total) hydroxyl groups does not practically change [50% (pH 6.l), 48% (pH 4.9)] although the surface concentration of $W^{(vi)}$ increases considerably [5.66 (pH 6.l), 7.35 (pH 4.9) μmol $W^{(vi)}$ m^{-2}].

In view of this let us speculate about the $W^{(vi)}$ species formed in the calcined samples. There are of course, several possibilities. The most important are visualized below.

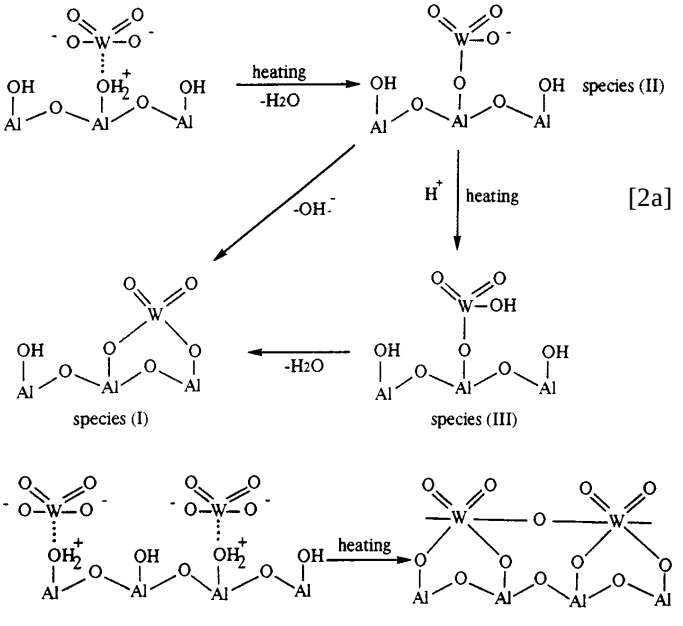

Although it is not possible to know the relative extent of each of the processes [2a] and [2b], some evidence may be drawn from our DRS results. Inspection of Fig. 8 shows an increase of the $W^{(vi)}$ in octahedral symmetry when the $W^{(vi)}$ increased from 13.9 to 17.3% WO_3 and this may reflect the formation of the polymeric $W^{(vi)}$ mentioned above. However, the extent to which process [2b] takes place seems to be insufficient to disturb the linearity in the increase of the tetrahedral $W^{(vi)}$ (see Fig. 8). That both processes [2a] and [2b] result in a monolayered structure for the supported

$W^{(vi)}$ phase is in excellent agreement with our BET. XPS, and XRD results taken for the EDF samples with $W^{(vi)}$ content in the range 3.3–17.3% WO_3.

The deposition of the $W^{(vi)}$ through the adsorption of the *polymeric* $HW_6O_{20}(OH)_2^{5-}$ species at pH 4.0 and 3.5 caused a decrease in the tetrahedral $W^{(vi)}$, an increase in the octahedral $W^{(vi)}$, as well as the formation of supported WO_3 crystallites in full agreement with our XPS and XRD results and the considerations stated in the preceding paragraphs.

Comparing the DR results obtained for the EDF catalyts with the corresponding ones obtained for the NDI catalysts, it is interesting to note the relatively low tetrahedral $W^{(vi)}$ in the later. Taking into account the mode of deposition in the NDl catalysts, this is rather expected and should be related with the relatively low dispersity obtained in these catalysts.

Let us now give the most important conclusions drawn from the joint use of BET, XPS, XRD, and DRS:

(i) Concerning the EDF catalysts it may be concluded that a close relation exists between the *nature* of the deposited $W^{(vi)}$ species on the surface of γ-alumina and *the structure and dispersity* of the $W^{(vi)}$ supported phase: Deposition via the monomeric WO_4^{2-} species provides a well-dispersed, presumably monolayered, $W^{(vi)}$ phase relatively rich in tetrahedral $W^{(vi)}$. In contrast deposition via the polymeric $HW_6O_{20}(OH)_2^{5-}$ species results in a supported phase with relatively low dispersity and a relatively small amount of tetrahedral $W^{(vi)}$. Supported WO_3 crystallites with size greater than 40 nm are formed in this case.

(ii) The mode of deposition, adsorption, and reaction in the case of EDF and precipitation in the case of NDI catalysts is closely related with the structure and dispersity of the supported $W^{(vi)}$ phase. As was expected, precipitation resulted in a supported phase with relatively low dispersity and relatively poor tetrahedral $W^{(vi)}$.

Temperature-Programmed Reduction

Taking into account our DRS results and the considerations of the previous paragraphs one might be inclined to believe that the nature, but not the dispersity, of the supported $W^{(vi)}$ species in the calcined samples depends slightly on the mode of deposition [adsorption vs reaction] of the WO_4^{2-} species. In fact, adsorption could resulted to the polymeric species via process (b) in addition to the monomeric or dimeric ones [species (I), (III), and (IV)]. However, as already mentioned, the joint use of BET, XPS, XRD, and DRS cannot help us to elucidate this point. To do that we employed two additional techniques: TPR and NO chemisorption.

Let us start with TPR. The reduction behavior of the WO_3/γ-Al_2O_3 catalysts mainly prepared by the classical dry or nondry impregnations has been intensively studied (14, 21, 22, 24, 27, 34). In most cases, TPR and XPS were used. Figure 9 illustrates the TPR curves of the specimens

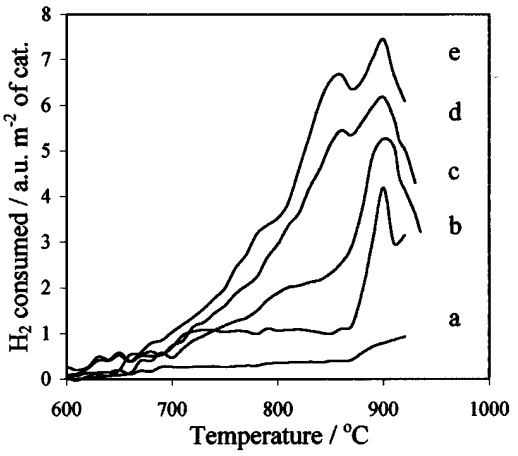

FIG. 9. Temperature-programmed reduction curves of the specimens prepared by EDF at various pH's. (a) 3.3% WO_3 (pH 7.0), (b) 11% WO_3 (pH 7.4), (c) 17.3% WO_3 (pH 4.9), (d) 19.9% WO_3 (pH 4.0), (e) 21.2% WO_3 (pH 3.5).

prepared by EDF at various pH. A peak centered at about 900°C is observed in all the specimens studied. This may be attributed to the reduction of well-dispersed supported monolayer rich in tetrahedral $W^{(vi)}$ (see for example Fig. 1b of Ref. (22)). This peak has been observed at 1000°C by Vermaire and Van Berge (34). Taking into account that their samples were also prepared by EDF, we have for the moment no plausible explanation for this difference. Our assignment was corroborated by recording the TPR curve of a mechanical mixture of γ-Al_2O_3 and Na_2WO_4, where the $W^{(vi)}$ is in tetrahedral symmetry. The maximum reduction was, in effect, observed at 900°C . An additional reduction peak centered at about 860°C is, moreover, observed at the specimens where WO_3-supported crystallites have been detected by XRD. Therefore, this peak, greater in the sample with the maximum $W^{(vi)}$ content, would be attributed to the supported WO_3. In the TPR curve recorded for the unsupported WO_3 we detected a very intense reduction peak at about 890°C and this corroborated the assignment mentioned. It should be noted that a reduction peak centered at about 835°C has been also detected by Vermaire and Van Berge (34) for an EDF WO_3/γ-Al_2O_3 where the $W^{(vi)}$ monolayer had been completed. Let us concentrate our attention on the TPR curve corresponding to the specimen with $W^{(vi)}$ content equal to 17.3% WO_3, which has been prepared at pH 4.9. A shoulder centered at about 800°C, which is absent in the TPR curves of the specimens with $W^{(vi)}$ content equal to 3.3, 11, and 13.9%, prepared in the pH range 7.4–6.1 may be seen. It should be remembered that from the preparative point of view the main difference between the sample prepared at pH 4.9 and those prepared in the pH range 7.4–6.1 is that in the first case the deposition takes place almost exclusively *by adsorption* of the WO_4^{2-} ions on sites created in the IHP by single $AlOH_2^+$

groups whereas in the latter case the deposition takes place almost exclusively *by reaction* of the WO_4^{2-} ions with one or two $AlOH_2^+$ groups. It was, moreover, speculated that the formation of the polymeric $W^{(vi)}$ species via the process (b) in the first case in addition to species (I), (III), and (IV) formed almost exclusively in the second case. Could we attribute the observed shoulder to the polymeric $W^{(vi)}$ species. It cannot be excluded. Therefore, the TPR curves offer evidence, indeed too weak evidence, that the mode of the WO_4^{2-} deposition is reflected in the reactivity of the supported $W^{(vi)}$ monolayer. However, we return to this point when we discuss the NO chemisorption results. Figure 10 illustrates the TPR curves for the EDF specimens with the $W^{(vi)}$ equal to 3.3, 11, and 21.2% WO_3 and for the NDI specimens with the corresponding $W^{(vi)}$ loadings. It may be seen that in all cases the supported $W^{(vi)}$ is more reducible in the NDI specimens. This is manifested both by the intensity of the reduction bands and by the temperature where these bands appear. The above observation may be attributed to the relatively low dispersity of the $W^{(vi)}$ phase, relatively poor in tetrahedral $W^{(vi)}$, in the NDI specimens. In fact, this situation implies relatively low "supported phase-support" interactions resulting in an increase in the $W^{(vi)}$ reducibility. Therefore, the TPR results corroborated the second conclusion of the preceding paragraph drawn from the BET, XPS, XRD, and DRS results.

NO Chemisorption

Let us now present our NO chemisorption results. It is well known that NO chemisorbed per gram of an unpromoted $Mo^{(vi)}$- or $W^{(vi)}$-supported catalyst may be used as a measure of the surface of the supported ion (37). In this respect this technique is expected to provide results similar with those provided by XPS. However, there are two important differences: (i) NO chemisorption is limited to the first molecular layer and (ii) XPS and NO chemisorption exhibit different sensitivities concerning the "supported phase-carrier" interactions. Therefore, XPS and NO results are expected simply to indicate similar trends although these might be different in details. Figure 11 illustrates the variation with the $W^{(vi)}$ loading of the NO chemisorbed per gram of the catalysts examined in the present study. The most important observation is that the amount of the NO chemisorbed on the EDF samples is greater than that of the NO chemisorbed on the corresponding NDI samples. This is in full agreement with our picture obtained so far that the supported phase in the EDF samples is better dispersed, more strongly interacted with the support surface, and more rich in $W^{(vi)}$ tetrahedral than that of the corresponding NDI specimens.

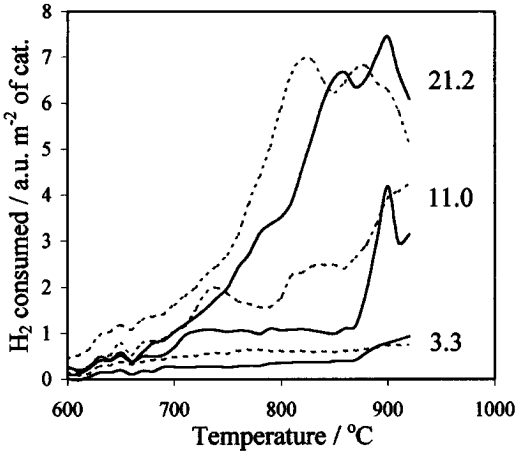

FIG. 10. Temperature-programmed reduction curves of the specimens with $W^{(vi)}$ loading equal to 3.3, 11, and 21.2% WO_3 prepared by EDF (—) and NDI (- - -). The values of the $W^{(vi)}$ loading are indicated.

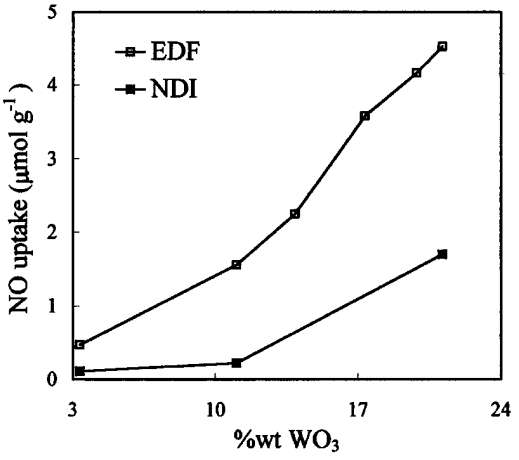

FIG. 11. Variation, with the $W^{(vi)}$ loading, of the amount of the chemisorbed NO per gram of the catalysts studied.

A second quite important observation is the abrupt increase in the amount of NO chemisorbed when the loading of the EDF sample increased from 13.9 to 17.3% WO_3. This transition is not present in the XPS curve (see Fig. 2) but it corresponds to the change in the TPR curve for the same increase in the $W^{(vi)}$ loading. The latter had been offered as evidence that the deposition of the WO_4^{2-} ions by adsorption would result in polymeric $W^{(vi)}$ species in addition to species (I), (III), and (IV) formed when the surface reaction is the unique deposition process. Our NO chemisorption results corroborate, thus, this statement.

Finally, it should be noted that the decrease in the slope of the EDF curve as the $W^{(vi)}$ loading increases from 17.3% WO_3 to 21.3% WO_3 should be related wfth the decrease in the $W^{(vi)}$ dispersity in this range (see Fig. 2).

Temperature-Programmed Desorption of Ammonia

It is well known that the WO_3/γ-Al_2O_3 catalysts display acidic properties (28–33). A critical question raised

is whether the method followed for depositing the $W^{(vi)}$ species on the support surface has an influence on the acidic properties of the WO_3/γ-Al_2O_3 samples determined after calcination. The temperature-programmed desorption of ammonia (NH_3-TPD) was employed as a qualitative probe for the overall acid site strength (28). Figure 12 shows the NH_3-TPD results for γ-Al_2O_3 and the EDF samples. The EDF and NDI samples with the minimum $W^{(vi)}$ content showed almost identical NH_3-TPD curves with that of the support. It may be observed that in all samples, ammonia desorbs in one large envelope centered at about 150°C and this is in excellent agreement with the literature (28). The deposition of the $W^{(vi)}$ species causes a shift of the maximum to lower temperatures (10–15°C) indicating the creation of relatively weak acid sites. Another observation is that the deposition of the $W^{(vi)}$ species depresses the strongest acidic centers of the γ-alumina, which hold ammonia in the temperature range 400–500°C. Finally, it may be observed that increase in the $W^{(vi)}$ loading up to 19.9% WO_3 causes an increase in the total number of acid sites as it is estimated by the area below the NH_3-TPD curves in the range 0–500°C. Further increase in the $W^{(vi)}$ loading brings about a decrease in the total number of acid sites. We attribute this phenomenon to the relatively high extent of formation ot supported WO_3 crystallites on expense of the $W^{(vi)}$ supported monolayer and the subsequent decrease in the dispersity of the supported $W^{(vi)}$ (See Fig. 2).

Figure 13 illustrates the NH_3-TPD curves achieved for the EDF and NDI specimens with $W^{(vi)}$ content equal to 11% WO_3 and 21.3% WO_3. Comparison of the NH_3-TPD curves of the specimens with $W^{(vi)}$ loading equal to 11% WO_3 shows that EDF provided a more acidic catalyst than that provided by NDI. In fact, the number and the strength of the acidic sites is greater in the EDF than in the NDI catalyst. This might be related to the very good dispersity

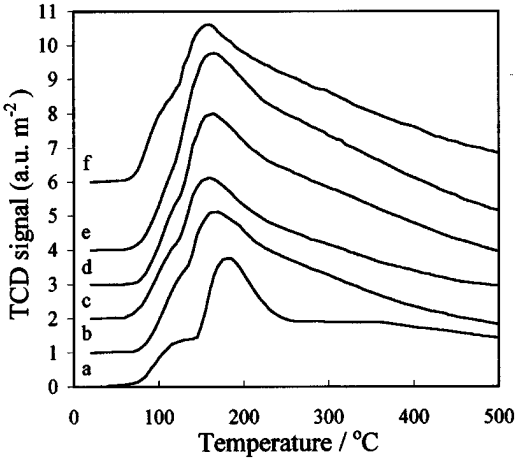

FIG. 12. Temperature-programmed desorption, of NH_3 curves for the γ-Al_2O_3 and the EDF sainples: (a) γ-Al_2O_3, (b) 11% WO_3, (c) 13.9% WO_3, (d) 17.3% WO_3, (e) 19.9% WO_3, and (f) 21.2% WO_3.

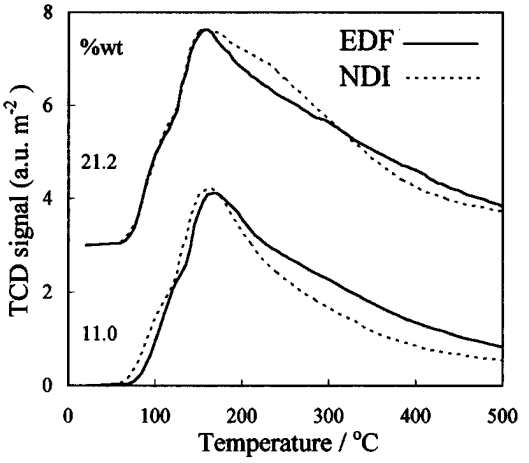

FIG. 13. Temperature-programmed desorption of NH_3 curves for the EDF and NDI specimens with $W^{(vi)}$ content equal to 11% WO_3 and 21.2% WO_3.

and the relatively strong "active phase-carrier interaction" achieved in the EDF specimen. Comparison of the NH_3-TPD curves for the specimens with the maximum $W^{(vi)}$ content shows that EDF provides more numerous strong acid sites, although the total number of these sites is approximately the same. It should be noted that even in the samples with the minimum $W^{(vi)}$ loading, EDF provided a catalyst with a slightly larger number of acid sites than NDI. *In conclusion EDF results in more acidic WO_3/γ-Al_2O_3 catalysts than NDI.*

Microelectrophoresis

Useful information concerning acidity may be drawn from the study of the microelectrophoretic curves of the samples. These depict the variation of the microelectrophoretic mobility (U_X) of the sample particles with pH. The value of U_X is proportional to the charge in the shear plane of the double layer developed between the surface of the sample particles and the solution. Positive (negative) values for the U_X indicate positive (negative) values for the charge in the shear plane, which in turn indicates positive (negative) charge on the surface provided that no considerable specific adsorption takes place (2). However, in any case the microelectrophoretic curves may be used just to investigate the *trend* for a series of samples to be charged positively or negatively by protonating or deprotonating their surface hydroxyls.

Figure 14 illustrates the microelectrophoretic curves for γ-alumina and some EDF samples. It was not possible to obtain these curves for the NDI specimens with $W^{(vi)}$ content equal to 11 and 21.2% WO_3 because in these cases it was observed that *a portion of the $W^{(vi)}$-supported phase was diluted in the solution used*. This is in full agreement with our conclusion drawn from the present study that the supported phase in the NDI samples is weakly bounded on

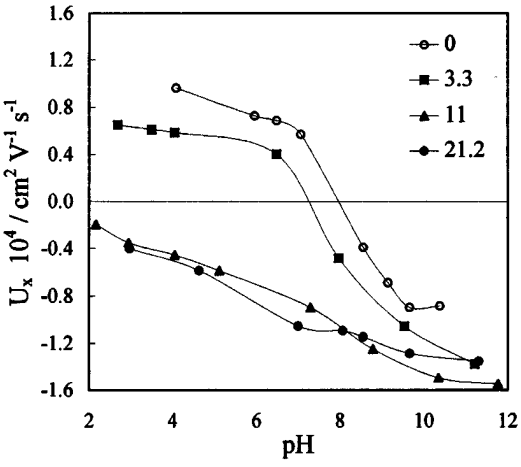

FIG. 14. Variation of the microelectrophoretic mobility with the pH of the solution for γ-alumina and some EDF samples. (○) γ-Al_2O_3, (■) 3.3% WO_3, (▲) 11% WO_3, and (●) 21.2% WO_3.

the support surface compared with that formed in the corresponding EDF samples. Inspection of Fig. 14 shows a shift of the isoelectric point (IEP) to lower pH value when the minimum amount of $W^{(vi)}$ was added on the support surface. A similar curve was obtained for the corresponding NDI specimen. This clearly shows an increase in the acidity even for the specimens with the minimum $W^{(vi)}$ content and indicates the sensitivity of the methodology to small increments of the acidity relative to the support. Increase in the $W^{(vi)}$ content from 3.3 to 11% WO_3 changes drastically the microelectrophoretic curve. Now the values of U_X are negative over the whole pH range studied and this indicates considerable increase in the acidity. Further increase in the $W^{(vi)}$ content does not change considerably the microelectrophoretic curve. Thus, the curve achieved for the sample 2l.2% WO_3/γ-Al_2O_3 is similar to that achieved for the sample 11% WO_3/γ-Al_2O_3 and this shows that this technique is not too sensitive to investigate small differences in the acidity when the acidity is quite high.

The study of the microelectrophoretic mobility curves has been used in the past in order to investigate the surface coverage of the γ-Al_2O_3 surface by the $W^{(vi)}$-supported phase. The methodology is supported on the underlying asumptions (31, 32):

(i) The supported phase is composed from WO_3 crystallites or the IEP of the supported phase is similar to that of the bulk WO_3.

(ii) The deposition of the $W^{(vi)}$ phase on the γ-alumina support does not disturb considerably the acid–base behavior of the uncovered support surface.

Under the above assumptions a progressive shift with the $W^{(vi)}$ loading of the IEP toward the IEP of the WO_3 (≈ 0.3) (31, 45–47) should be observed. Our experiments show that, at least under our experimental conditions, this is not the case. This indicates that the aforementioned assumptions are not realistic for the system under study in agreement with our characterization results.

Catalytic Tests and Carbon Deposition

The physicochemical characterization described in the previous sections strongly suggested that the EDF samples should be more active than the corresponding NDI specimens. In the present work we report only few catalytic results just to investigate this point, although a systematic comparison concerning the hydrodesulfurization activity of these two series will be reported in the next, final, article of this series dealing with the physicochemical characteristics and the catalytic behavior of the Ni-promoted EDF and NDI catalysts.

Figures 15 and 16 illustrate, respectively, the hydrodesulfurization and hydrogenation activity achieved for some EDF and NDI catalysts. It may be seen that in all cases the EDF samples are more active than the corresponding NDI samples. This is another example that shows that EDF is a promising methodology for preparing supported catalysts. However, much more experimentation is needed in order to be sure that the EDF samples are better from the viewpoint of catalysis than from the corresponding NDI samples. For instance, the relatively high acidity of the EDF samples is expected to facilitate the coke formation during hydrodesulfurization. This is, in effect, the case as may be observed in Fig. 17.

Differential Thermogravimetry

The differences in the physicochemical, and therefore in the catalytic properties, of the EDF and the corresponding NDI samples discussed so far were interpreted in terms of the mode of deposition. Specifically it was assumed that

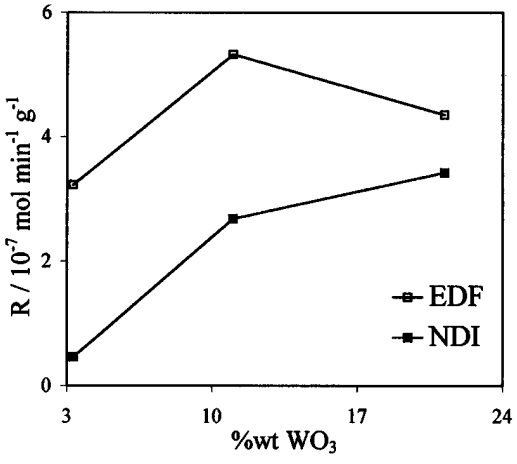

FIG. 15. Hydrodesulfurization activity achieved for some EDF and NDI catalysts at 375°C . The hds of thiophene has been used as a probe reaction.

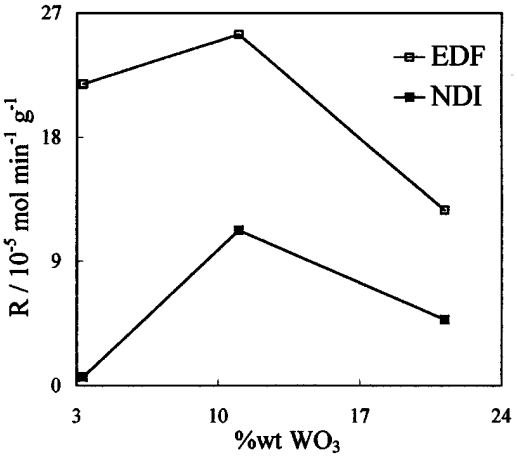

FIG. 16. Hydrogenation activity achieved for some EDF and NDI catalysts at 375°C. The hydrogenation of cyclohexene has been used as a probe reaction.

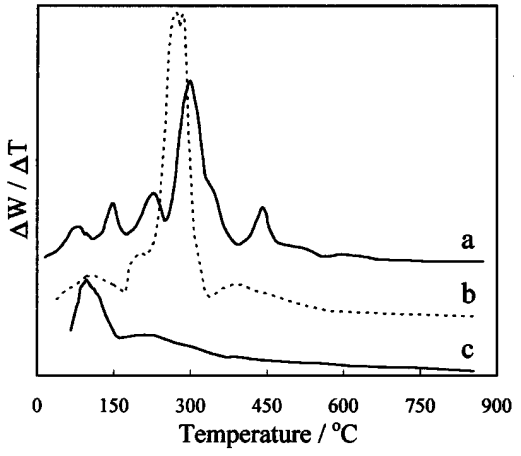

FIG. 18. Differential thermogravimetry curves for $(NH_4)_{12}W_{12}O_{41}$ $5H_2O$ and two NDI specimens (a) $(NH_4)_{12}W_{12}O_{41}5H_2O$, (b) 21.1% WO_3, and (c) 11% WO_3.

whereas in the EDF samples the $W^{(vi)}$ is deposited by adsorption or surface reaction in the step of impregnation (see Fig. 1), in the NDI samples a large portion of the $W^{(vi)}$ is deposited by precipitation in the step of drying, which follows impregnation. The first part of this assumption does not need any verification (see Fig. 1) but the second one should be further investigated. A simple methodology for approaching this point is to study the DTGA curves of model compounds and samples before calcination.

Figure 18 illustrates the DTGA curves of the $(NH_4)_{12}W_{12}O_{41}5H_2O$ used for the preparation of the $W^{(vi)}$ impregnating solutions as well as the DTGA curves of the NDI specimens with $W^{(vi)}$ loading equal to 11 and 21.2% WO_3. In the DTGA curve of the model compound appear five peaks. The first one appearing at about 85°C is attributed to the removal of the physically adsorbed water.

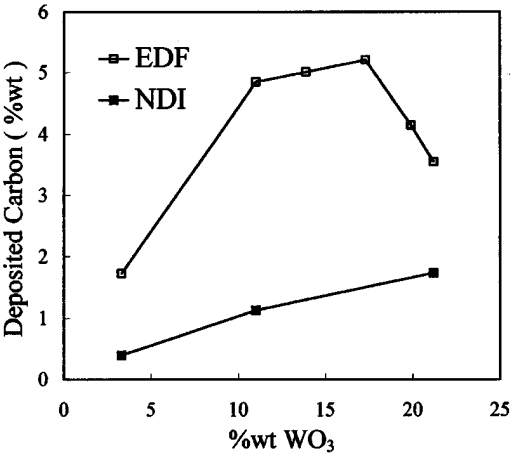

FIG. 17. Coke formation on the surface of some EDF and NDI samples during aging and catalytic testing in hds and hydrogenation process.

The second and third peaks appearing at 155 and 235°C correspond to the removal of 4 and 1 water molecules, respectively, derived from the decomposition of the salt. The intense band centered at about 310°C is due to the removal of 12 NH_4^+ ions. Finally the peak at 450°C corresponds to the removal of 5 O atoms. The above assignments were based on the literature (44). Moreover, they are in full agreement with our calculations based on the decrease in the weight corresponding to each peak. The thermal process so described corresponds to the formation of $W_{12}O_{36}$=WO_3. In fact, at the end of the process the solid had the characteristic yellow color of WO_3 at 900°C.

The DTGA curve of the 21.2% WO_3/γ-Al_2O_3 NDI sample, taken before calcination (23.5% ammonium tungstate/γ-Al_2O_3) is similar to that obtained for the ammonium tungstate. In fact, five peaks also appeared but at temperatures lower than those cdrresponding to the ammonium tungstate. This may be attributed to the very large specific surface area of the catalyst, compared with that of the ammonium tungstate, and therefore to the easier contact of the surface with the atmospheric air. Calculation of the decrease in the weight corresponding to peaks 2–5 is in good agreement with the decomposition of the supported ammonium tungstate. This is strong evidence that the $W^{(vi)}$ surface compound formed on the γ-alumina during the NDI process has similar stoichiometry with the ammonium tungstate. Going from the specimen 21.2% WO_3/γ-Al_2O_3 to the specimen 11% WO_3/γ-Al_2O_3 the DTGA curve is changed considerably. However, the decrease in the weight corresponding to the second very large peak centered at about 230°C (ending at about 550°C) corresponds to the transformation of the ammonium tungstate into tungsta. The peak that appeared at 110°C is attributed to the removal of the physically adsorbed water. Concerning the NDI specimen with the minimum $W^{(vi)}$ content, the DTGA

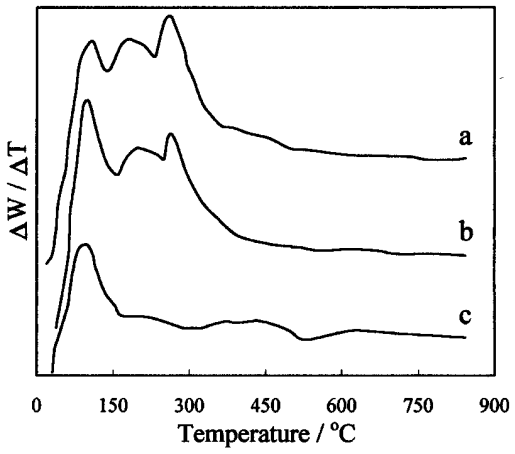

FIG. 19. Differential thermogravimetry curves for three EDF samples (a) 21.2% WO_3, (b) 11% WO_3, and (c) 3.3% WO_3.

curve showed the peak at 110°C attributed to the physically adsorbed water as well as a hardly detectable peak in the range 150–500°C. The decrease in the weight concerning this peak corresponded to the decomposition of the ammonium tungstate. In conclusion the study of the DTGA curves of the NDI specimens corroborated our assumption that a large portion of the $W^{(vi)}$ is deposited on the γ-alumina surface by precipitation in the step of drying.

Figure 19 illustrates the DTGA curves of three EDF samples (3.3, 11, and 21.3% WO_3). These are quite similar to each other but are quite different than the DTGA curve of the ammonium tungstate. Three main peaks are observed: The first centered at about 100–110°C, may be attributed to the removal of the physically adsorbed water. The second and third peaks could be attributed to the various $W^{(vi)}$ species deposited on the γ-alumina surface as well as to the decomposition of the NH_4NO_3 presumably formed during drying. Although it is quite difficult to assign these peaks to the decomposition of a given $W^{(vi)}$ species formed on the γ-alumina surface during impregnation it may be stressed that the pronounced differences between the DTGA curves of the EDF specimens with the DTGA curves of the corresponding NDI specimens corroborate our assumption that different mode of deposition (precipitation vs adsorption, reaction) is followed in each case.

CONCLUSIONS

The most important findings drawn from the present study may be summarized as follows:

1. Deposition through adsorption or surface reaction of the monomeric WO_4^{2-} species in the pH range 7.4–4.9 resulted in a well-dispersed, presumably monolayer, $W^{(vi)}$ phase relatively rich in tetrahedral $W^{(vi)}$. In contrast, deposition through adsorption of polymeric $HW_6O_{20}(OH)_2^{5-}$ species, at pH 4 and 3.5, resulted in a supported phase with relatively low dispersity and a relatively small amount of tetrahedral $W^{(vi)}$. Supported WO_3 crystallites with size greater than 40 nm were detected in these cases.

. The change in the deposition mechanism (upon decreasing pH from 6.1 to 4.9) from deposition through surface reaction of the WO_4^{2-} species with the neutral hydroxyls of the support into deposition through adsorption of these species on protonated hydroxyls of the support brought about decrease in the "supported phase-carrier" interactions and increase in the surface of the supported $W^{(vi)}$.

3. NDI resulted in a supported phase with lower $W^{(vi)}$ dispersity and tetrahedral $W^{(vi)}$ less rich than EDF. Moreover, the acidity of the NDI samples is lower than that of the corresponding EDF samples.

4. EDF provided more active catalysts than NDI with respect to the hds of thiophene and the hydrogenation of cyclohexene.

ACKNOWLEDGMENTS

We gratefully acknowledge experimental assistance by Mr. A. Tzanos and Mr. S. Kravaritis.

REFERENCES

1. Karakonstantis, L., Bourikas, K., and Lycourghiotis, A., Submitted to this Journal.
2. Karakonstantis, L., Kordulis, Ch., and Lycourghiotis, A., *Langmuir* **8**, 1318 (1992).
3. Iannibello, A., and Mitchell, P. C. H., "Preparation of Catalysts" (B. Delmon, P. Grange, P. A. Jacobs, and G. Poncelet, Eds.), Vol. II, p. 469. Elsevier, Amsterdam, 1979.
4. Iannibello, A., Villa, P. L., and Marengo, S., *Gazz Chim. Ital.* **109**, 521 (1979).
5. Iannibello, A., Marengo, S., Trifiro, F., and Villa, P. L., "Preparation of Catalysts" (B. Delmon, P. Grange, P. A. Jacobs, and G. Poncelet, Eds.), Vol. II, p. 65, Elsevier, Amsterdam, 1979.
6. Iannibello, A., Marengo, S., and Villa, P. L., "Proceedings, International Conference on the Chemistry and Uses of Molybdenum, (H. F. Barry and P. C. H. Mitchell, Eds.), Climax Molybdenum Co, Ann Arbor," p. 92, 1979.
7. Tittarelli, P., Iannibello, A., and Villa, P. L., *J. Solid State Chem.* **37**, 95 (1981).
8. Thomas, R., Mittelmeijer-Hazeleger, F. P., Kerkhof, J. M., Moulijn, J. A., Medema, J., and De Beer, V. M. J., *in* "Proceedings, International Conference on the Chemistry and Uses of Molybdenum, (H. F. Barry and P. C. H. Mitchell, Eds.), Climax Molybdenum Co, Ann Arbor," p. 85, 1979.
9. Wang, L., and Hall, W. K., *J. Catal.* **77**, 232 (1982).
10. Salvati, L. Jr., Makovski, L. E., Stencel, J. M., Brown, F. R., and Hercules, D. M., *J. Phys. Chem.* **85**, 3700 (1981).
11. Chan, S., Wachs, I. F., Murrell, L. L., Wang, L., and Hall, W. K., *J. Phys. Chem.* **88**, 5831 (1984).
12. Thomas, R., Moulijn, J. A., and Kerkhof, J. M., *Recl. Trav. Chim. Paybas* **96**, M134 (1977).
13. Thomas, R., Kerkhof, J. M., Moulijn, J. A., Medema, J., and De Beer, V. H. J., *J. Catal.* **61**, 558 (1980).
14. Thomas, R., De Beer, V. H. J., and Moulijn, J. A., *Bull Soc. Chim. Belg.* **90**, 1349 (1981).
15. Chan, S. S., Wachs, I. F., and Murrell, L. L., *J. Catal.* **90**, 150 (1984).

16. Chan, S. S., Wachs, I. F., and Murrell, L. L., and Dispenziere, N. C., *J. Catal.* **92**, 1 (1985).
17. Chan, S. S., Wachs, I. F., Murrell, L. L., and Dispenziere, N. C., *in* "Catalysis on the Energy Scene" (S. Kaliaguine and A. Mahay, Eds.). Elsevier, Amsterdam, 1984.
18. Biloen, P., and Pott, G. T., *J. Catal.* **30**, 169 (1973).
19. Wachs, I. E., Chersish, C. C., and Hardenberg, J. H., *Appl. Catal.* **13**, 335 (1985).
20. Stencel, J. M., Makovsky, L. E., Diehl, J. R., and Sarkus, T. A., *J. Raman Spectrosc.* **25**, 282 (1984).
21. Chappell, P. J. C., Kibel, M. H., and Baker, B. G., *J. Catal.* **110**, 139 (1988).
22. Scheffer, B., Molhoek, P., and Moulijn, J. A., *Appl. Catal.* **46**, 11 (1989).
23. Scheffer, B., Mangnus, P. J., and Moulijn, J. A., *J. Catal.* **121**, 18 (1990).
24. Grunert, W., Shpipo, E. S., Feldhaus, R., Anders, K., Antoshin, G. V., and Minachev, K. H. M., *J. Catal.* **107**, 522 (1987).
25. Grunert, W., Morke, W., Feldhaus, R., and Anders, K., *J. Catal.* **117**, 485 (1989).
26. Chan, S. S., Wachs, I. E., and Murrell, L. L., *J. Catal.* **90**, 150 (1984).
27. Thomas, R., Van Oers, E. M., De Beer, V. H. J., Medema, J., and Moulijn, J. A., *J. Catal.* **76**, 241 (1982).
28. Soled, S. L., Mc Vicker, G. B., Murrell, L. L., Sherman, L. G., Dispenziere, N. C. Jr., Hsu, S. L., and Waldman, D., *J. Catal.* **111**, 286 (1988).
29. Bernholc, J., Horsley, J. A., Murrell, L. L., Sherman, L. G., and Soled, S., *J. Phys. Chem.* **91**, 1526 (1987).
30. Soled, S. L., Murrell, L. L., Wachs, I. E., Mc Vicker, G. B., Sherman, L. G., Chan, S. S., Dispenziere, N. C., and Baker, R. T. K., *in* "Solid State Chemistry in Catalysis" (R. K. Grasselli and J. F. Brazdil, Eds.), ACS Symp. Ser. No. 279. American Chemical Society, Washington, DC, 1985.
31. Llambias, F. G., Salvatierra, J., Bauyssieres, L., and Escudey, M., *Appl. Catal.* **59**, 185 (1990).
32. Brady, R. L., Southmayd, D., Contescu, C., Zhiang, R., and Schwarz, J. A., *J. Catal.* **129**, 195 (1991).
33. Zhang, R., Jagiello, J., Hu, J. F., Huang, Z. Q., Schwarz, G. A., and Datye, A., *Appl. Catal.* **19**, 123 (1992).
34. Vermaire, D. C., and Van Berge, P. C., *J. Catal.* **116**, 309 (1989).
35. Marczernko, Z., "Spectrophotometric Determination of Elements" (G. G. Ramsay, Translation Ed.), p. 569. Wiley, New York, 1970.
36. Spanos, N., Matralis, H. K., Kordulis, Ch., and Lycourghiotis, A., *J. Catal.* **136**, 432 (1992).
37. Papadopoulou, Ch., Lycourghiotis, A., Grange, P., and Delmon, B., *Appl. Catal.* **38**, 255 (1988).
38. Papadopoulou, Ch., Matralis, H. K., Lycourghiotis, A., Grange, P., and Delmon, B., *J. Chem. Soc. Faraday Trans.* **89**, 3157 (1993).
39. Quafi, D., Mauge, F., Lavalley, J. C., Payen, E., Kasztelan, S., Houan, M., Grimblot, J., and Bonnelle, J. P., *Catal. Today* **4**, 23 (1988).
40. Kerkhof, F. P. J. M., and Moulijn, J. A., *J. Phys. Chem.* **83**, 1612 (1979).
41. Kerkhof, F. P. J. M., Moulijn, J. A., and Heeres, A., *J. Electron Spectrosc. Relat. Phenom.* **14**, 453 (1978).
42. Massoth, F. E., *Adv. Catal.* **27**, 265 (1978).
43. Iannibello, A., Marengo, S., Berti, V., Villa, P. L., and Trifiro, F., *J. Chem. Eng.* **55**, 747 (1977).
44. Horsley, J. A., Wachs, I. E., Broun, J. M., Via, G. H., and Hardcastle, F. D., *J. Phys. Chem.* **91**, 4014 (1987).
45. El Wakkad, S. E. S., and Rirk, H. A., *J. Phys. Chem.* **61**, 494 (1957).
46. Parks, G. A., and De Bruyn, P. L., *J. Phys. Chem.* **66**, 967 (1962).
47. Parks, G. A., *Chem. Rev.* **65**, 177 (l965).